



Ultrasonic electrodeposition of platinum nanoflowers and their application in nonenzymatic glucose sensors

M.Q. Guo^a, H.S. Hong^a, X.N. Tang^a, H.D. Fang^a, X.H. Xu^{a,b,*}

^a School of Materials Science and Engineering, Tianjin University, Tianjin 300072, PR China

^b Tianjin Key Laboratory of Composite and Functional Materials, Tianjin 300072, PR China

ARTICLE INFO

Article history:

Received 25 September 2011

Received in revised form

30 November 2011

Accepted 30 November 2011

Available online 28 December 2011

Keywords:

Platinum nanoflowers

Ultrasonic electrodeposition

Electrocatalytic activity

Nonenzymatic glucose sensors

ABSTRACT

In the present study, Pt nanoflowers were fabricated on the bare Au electrodes by using template-free ultrasonic electrodeposition method. Scanning electron microscopy, X-ray photoelectron spectroscopy, energy dispersive X-ray detector as well as X-ray diffraction were used for the characterization. It was found that Pt nanoflowers were composed of metallic Pt. The electrocatalytic properties of the Pt nanoflowers electrode for glucose oxidation were investigated by cyclic voltammetry and differential pulse voltammetry. Cyclic voltammograms (CVs) results showed that the Pt nanoflowers electrode exhibited excellent catalytic activity towards glucose oxidation in neutral media. Differential pulse voltammograms (DPVs) results showed that at +0.03 V, the sensitivity of the electrode to glucose oxidation was $1.87 \mu\text{A cm}^{-2} \text{mM}^{-1}$ with a linear range from 1 mM to 16 mM and detection limit of 48 μM (signal-to-noise ratio of 3). In addition, the nonenzymatic glucose sensors exhibited excellent selectivity, stability and repeatability.

© 2011 Elsevier Ltd. All rights reserved.

1. Introduction

Diabetes mellitus is a worldwide public health problem. Hence development of sensing devices with high performance is very important for the diagnosis and management of diabetes mellitus [1]. Electrochemical glucose biosensors, especially amperometric biosensors, have been widely used because of its simple, accurate and fast analytical process [2]. Good selectivity and high sensitivity for glucose detection have been achieved by glucose enzymatic biosensors due to specificity of glucose oxidase [3–5]. However, the poor stability originated from the nature of the enzymes and the interference from some electro-oxidizable species remain as problems for real sensor applications [6,7]. In addition, reproducibility is still a critical issue in quality control, since the sensitivity of these glucose sensors essentially depends on the activity of the immobilized enzymes [6].

Direct electrocatalytic oxidation of glucose at a nonenzymatic electrode would exhibit conveniences and advantages to avoid the drawbacks of enzymatic sensors [8,9]. Many nonenzymatic glucose sensors have been explored, especially Pt-based amperometric glucose sensors [10]. However, these electrodes often have

drawbacks of low sensitivity and poor stability caused by surface poisoning from the adsorbed chloride ions and chemisorbed intermediates originated from glucose oxidation. In addition, such conventional electrodes often suffer from the interference from some electroactive species such as ascorbic acid (AA), uric acid (UA) and acetamidophenol (AAP) under physiological conditions [11–13].

Efforts have been attempted to overcome these drawbacks by taking advantage of nanostructured electrocatalysts with high active surface area, since nanostructured materials not only have high surface area but also can bring in unique catalytic properties to the materials [14,15]. Mesoporous Pt [16], highly ordered Pt nanotube arrays [17] and macroporous Pt templates [18] have been developed to enhance the amperometric response of glucose oxidation and lower the interference from the electroactive species. Bimetallic alloys are also widely used in catalysis and sensing fields due to their favorable properties in comparison with the corresponding monometallic counterparts such as high catalytic activity, catalytic selectivity and better resistance to deactivation such as Pt–Ti, Pt–Bi and Pt–Pb [19–22].

An ideal synthesis method of Pt-based electrocatalysts should be facile, cost-effective, controllable, reproducible and free of surface contaminants. In recent years, Pt-based alloy nanomaterials have been fabricated by a variety of strategies, such as hydrothermal and solvothermal techniques [23–25], solution–gel (sol–gel) process [26,27], physical synthesis [28,29], electrodeposition [14,30–32] and electroless deposition [33]. The hydrothermal and

* Corresponding author at: School of Materials Science and Engineering, Tianjin University, No. 72, Weijin Road, Tianjin 300072, PR China. Tel.: +86 22 27406127; fax: +86 22 27406127.

E-mail address: xhxu.tju@eyou.com (X.H. Xu).

solvochemical methods are easy and surfactant-free to fabricate Pt and Pt-based nanomaterials. However, these synthetic routes require elevated temperatures, relatively high loadings of Pt precursor, or polymeric stabilizers which may have undesired effects on the catalytic property of nanomaterials. In addition, most synthetic routes need a series of collection and wash steps which may further complicate the overall process [34,35].

The electrodeposition synthesis has been found to be a potentially superior method over other techniques due to the following advantages such as (1) single-step process at room temperature and relatively short process time; (2) effective control of size and shape of the particles; (3) easy to anchor securely on the substrate. Ultrasonic electrodeposition is a modified electrochemical approach, which takes full advantage of both electrodeposition method and ultrasonic treatment, and thus this fabrication approach shows large advantages in well-dispersed nanoparticles [36]. Results of literature search indicate that no study has been conducted to synthesize Pt nanoflowers by ultrasonic electrodeposition.

Accordingly, in the present study, we presented a one step, template-free approach for the preparation of Pt nanoflowers by ultrasonic electrodeposition. The morphology, composition and electrochemical properties of Pt nanoflowers were investigated by scanning electron microscopy (SEM), energy dispersive X-ray detector (EDX), X-ray photoelectron spectroscopy (XPS), X-ray diffraction (XRD), cyclic voltammetry, differential pulse voltammetry, and electrochemical impedance spectroscopy (EIS).

2. Materials and methods

2.1. Reagents

Chloroplatinic acid ($\text{H}_2\text{PtCl}_6 \cdot 6\text{H}_2\text{O}$) was purchased from Aldrich. Glucose was obtained from Kewei Chemical Reagent Co Ltd of Tianjin University (Tianjin, China). A 0.2 M phosphate buffer solution (PBS) was prepared using Na_2HPO_4 and NaH_2PO_4 . All aqueous solutions were prepared with reagent grade chemicals and double distilled water.

2.2. Apparatus

All the electrochemical measurements were performed on a PARSTAT 2263 electrochemical workstation (Princeton, USA). The electrochemical measurements were carried out with a conventional three-electrode system. A Pt nanoflowers electrode (4 mm diameter) was used as a working electrode with a platinum electrode (1 mm diameter) as an auxiliary electrode and a saturated calomel electrode (SCE) as a reference electrode in all cases (an Au electrode was used as the substrate electrode for the electrodeposition experiment. The electrodeposition set was shown in Scheme A in Supplementary material). Scanning electron microscope (FE-SEM, Hitachi S-4800), energy-dispersive X-ray analyzer (EDAX Genesis), X-ray photoelectron spectroscopy (PHL1600ESCA XPS) and X-ray diffractometer (XRD, RIGAKU/DMAX) were used to determine the morphology and composition of the samples. Electrochemical impedance spectroscopy (EIS) was measured in 5.0 mM $\text{K}_3[\text{Fe}(\text{CN})_6]/\text{K}_4[\text{Fe}(\text{CN})_6]$ (1:1) solution supported by 0.1 M KCl in the frequency range from 10^{-2} Hz to 10^5 Hz. Electrochemical catalytic behaviors of the electrodes towards glucose oxidation were characterized by cyclic voltammetry at a scan rate of 10 mV s^{-1} with the applied potential from -0.6 V to 0.9 V (versus SCE). All measurements were conducted at room temperature.

2.3. Preparation of Pt nanoflowers

Before electrodeposition, Au electrodes (4 mm diameter) were polished with 1.0, 0.3 and $0.05 \mu\text{m}$ alumina slurry, and then

ultrasonically cleaned in double distilled water and finally dried in air. The electrochemical deposition of Pt nanoflowers was performed in 0.5 M H_2SO_4 aqueous solution containing 3 mM H_2PtCl_6 at -0.02 V , -0.2 V and -0.6 V . During potentiostatic deposition, ultrasonic wave (45 W) irradiation was employed. The obtained Pt nanoflowers electrode was washed carefully with redistilled water and then dried at room temperature.

3. Results and discussion

3.1. Morphology, composition and structure analysis

The effect of electrodeposition potential on the morphology of Pt nanostructures was investigated by FESEM. SEM images of as-formed Pt nanostructures deposited at -0.02 V , -0.2 V and -0.6 V for 900 s were shown in Fig. 1. It was observed that distinct presence of Pt nanoflowers for the samples prepared at -0.2 V , while Pt nanoparticles were observed for the samples at -0.02 V and -0.6 V . Fig. 1(A) and (C) revealed that the Pt nanoparticles deposited at -0.6 V exhibited a higher distribution density and smaller diameter than those deposited at -0.02 V . Large particles and low distribution density were observed because of inadequate nucleation sites provided by the lower applied potential (-0.02 V). When the potential was increased to -0.2 V , high potential provided a sufficient driving force to promote the anisotropic growth of “petal” on the nanoflowers structure. When further increasing the potential (-0.6 V), it was deduced the inadequate Pt precursor in the solution during the later deposition period resulted in the formation of smaller particles with lower density.

The effect of electrolyte on the morphology was also investigated. From Fig. 1(B) and (D), it was observed that distinct presence of Pt nanoflowers with an average size of about 960 nm when using $\text{H}_2\text{SO}_4(0.5 \text{ M})/\text{H}_2\text{PtCl}_6(3 \text{ mM})$ as electrolyte. However, Pt nanoparticles were observed when using $\text{KCl}(0.5 \text{ M})/\text{H}_2\text{PtCl}_6(3 \text{ mM})$ as a replacement. According to the formation mechanism proposed by Du and co-workers [14], it could be deduced that the sulfuric acid ions in the electrolyte were preferentially absorbed on specific Pt surface planes, further growth of these specific crystal planes was inhibited, which resulted in the anisotropic growth of the material.

The kinetics of surface reactions on metals was extremely dependent on the morphology of the reacting surfaces. Real systems exhibited complicated shapes with a high degree of irregularity or disorder. In these cases, fractal geometry was useful to characterize rough surfaces in very general terms [37]. The fractal dimension was analyzed by using the box count method, and the results were shown in Fig. 2. The fractal dimension (D_f) could be obtained from the scaling relationship of $\text{Ln}(Nr) \propto D_f \cdot \text{Ln}(r)$. From Fig. 2(A) and (B), D_f of the Pt nanoflowers and Pt nanoparticles were calculated to be 1.737 and 1.703, respectively, which indicated that the surface of the Pt nanoflowers electrode was rougher than that of Pt nanoparticles electrode.

The dynamic growing processes of Pt nanoflowers were characterized by time-coursed SEM images (Fig. 3(A)–(D)). It was found that the quasi-spherical studded particles were initially formed at the earlier stages (Fig. 3(A)), which acted as the nuclei for subsequently producing Pt nanoflowers. When the deposition time reached to 300 s, many pricks started to form and extruded from the surfaces of the studded spherical particles (Fig. 2(B)). Further prolonging the growth time to 900 s, the perfect Pt nanoflowers were formed (Fig. 3(C)). After 900 s (Fig. 3(D)), the petals of Pt nanoflowers changed gradually, and became larger with the deposition time.

The composition and structure of Pt nanoflowers were examined by EDX, XPS and XRD. The EDX results in Fig. 4(A) showed that Pt element was exclusively observed. Fig. 4(B) showed the Pt 4f spectrum of Pt nanoflowers. As observed in Fig. 4(B), the

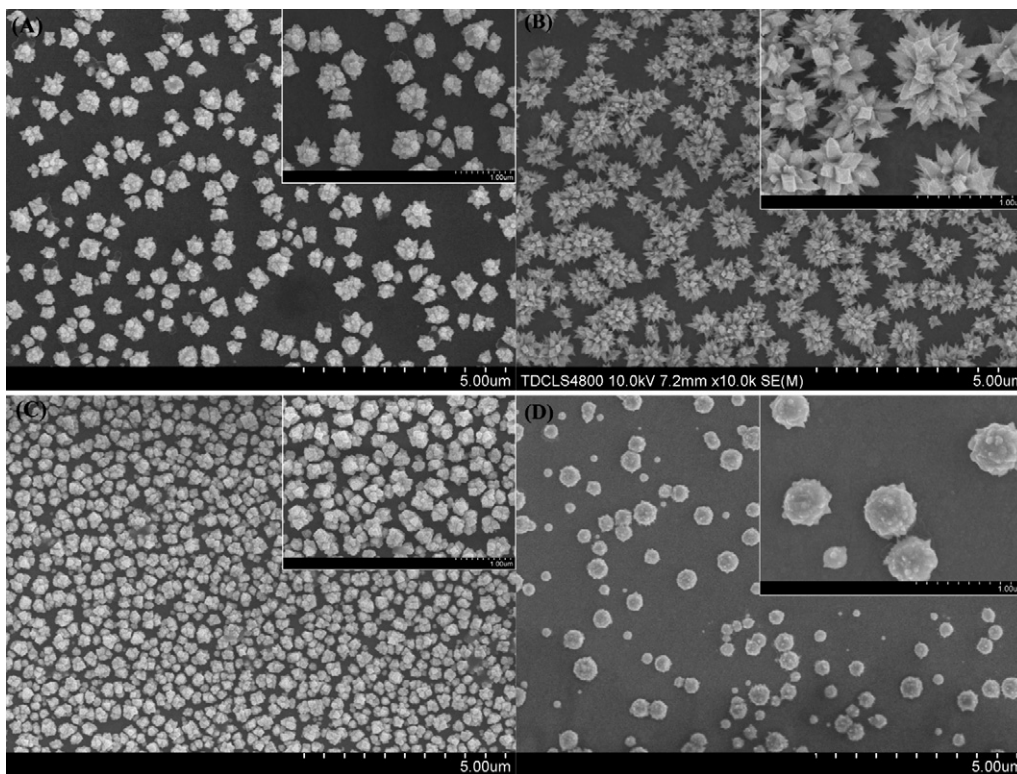


Fig. 1. SEM images of the samples electrodeposited in $\text{H}_2\text{SO}_4(0.5 \text{ M})/\text{H}_2\text{PtCl}_6(3 \text{ mM})$ for 900 s at (A) -0.02 V , (B) -0.2 V , (C) -0.6 V and (D) in $\text{KCl}(0.5 \text{ M})/\text{H}_2\text{PtCl}_6(3 \text{ mM})$ for 900 s at -0.2 V .

binding energies of Pt $4f_{7/2}$ and $4f_{5/2}$ electrons were 71.4 and 74.7 eV, respectively, which were in good agreement with pure bulk platinum. No XPS signal was associated with oxidized Pt species (such as Pt^{2+} and Pt^{4+}). This suggested that Pt nanoflowers were composed of metallic Pt. The structure of the samples was investigated by XRD. From XRD patterns for the Pt nanoflowers in Fig. 4(C), the well-defined peaks around 39.76° , 46.24° and 67.45° were attributed to the diffraction peaks of crystal faces Pt (1 1 1), (2 0 0) and (2 2 0), respectively.

3.2. Electrochemical characterization

The electroactive surface areas of the Pt nanoflowers and Pt nanoparticles electrode were estimated by the cyclic voltammetry method by using $\text{K}_3[\text{Fe}(\text{CN})_6]$ as a probe. Fig. 5 showed CVs of the Pt nanoflowers and Pt nanoparticles electrode in $\text{K}_3[\text{Fe}(\text{CN})_6](5 \text{ mM})/\text{KCl}(1 \text{ M})$ solution and the inset was the dependence of the peak current on the square root of the scan rate. From Fig. 5(A) and (B), it was observed that for both Pt nanoflowers electrode and Pt nanoparticles electrode, the peak current increased linearly with the square root of the scan rate,

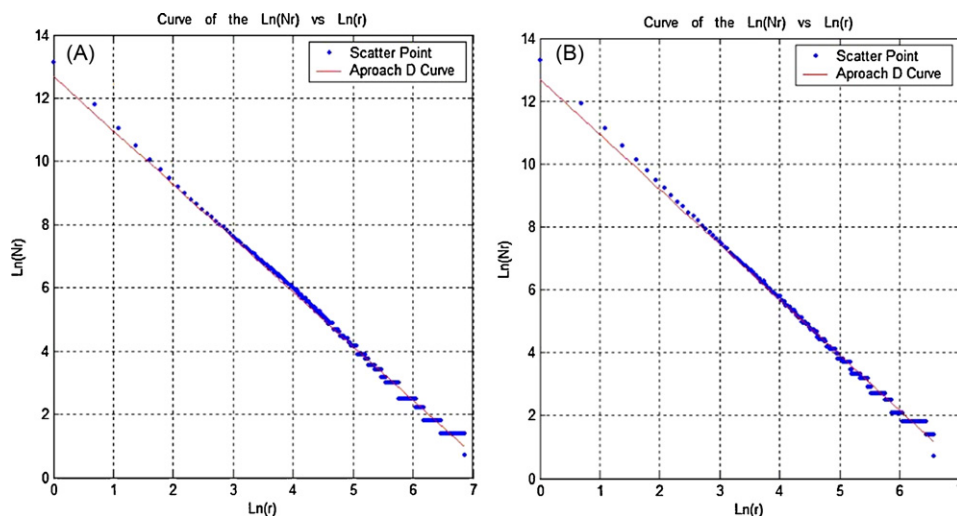


Fig. 2. Analysis of the fractal dimension of (A) Pt nanoflowers and (B) Pt nanoparticles by using the box count method.

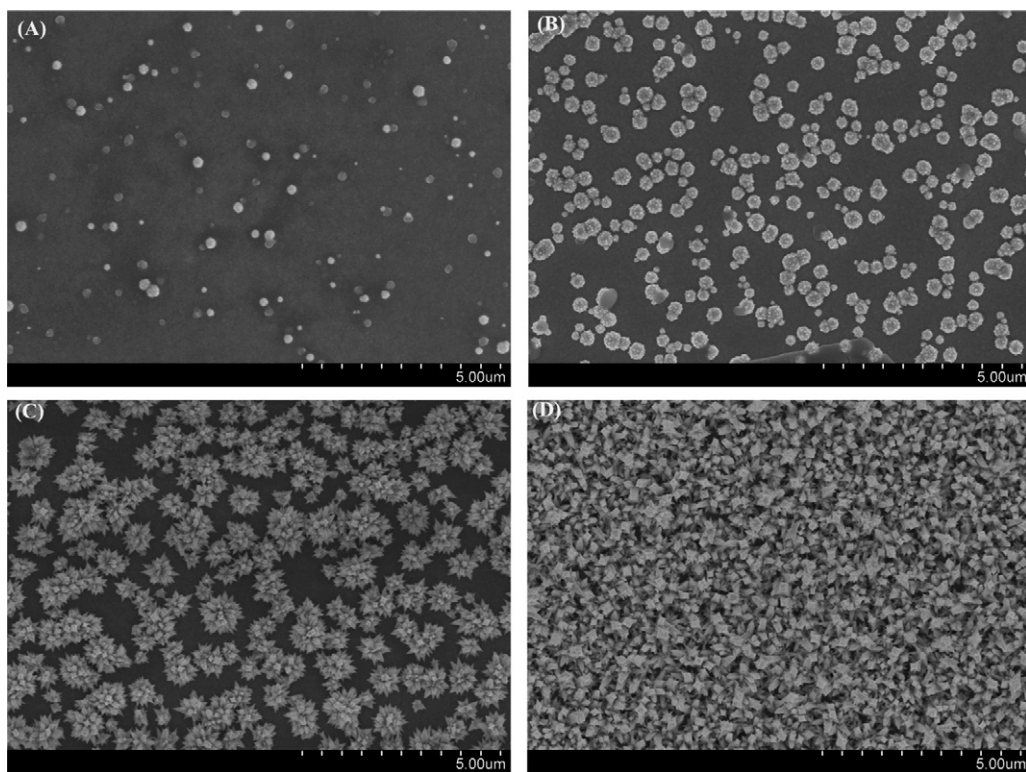


Fig. 3. SEM images of the samples electrodeposited in $\text{H}_2\text{SO}_4(0.5 \text{ M})/\text{H}_2\text{PtCl}_6(3 \text{ mM})$ at -0.2 V for (A) 30 s, (B) 300 s, (C) 900 s and (D) 3000 s.

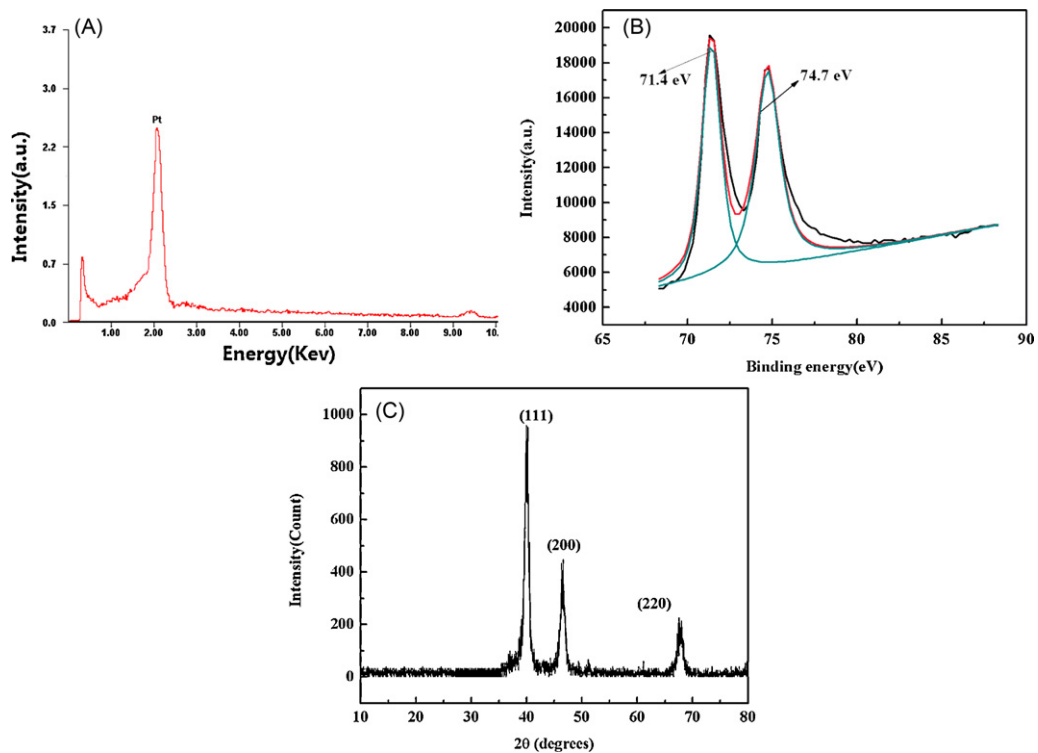


Fig. 4. (A) EDX spectrum of Pt nanoflowers, (B) XPS spectra of the Pt 4f regions for Pt nanoflowers and (C) XRD patterns of Pt nanoflowers.

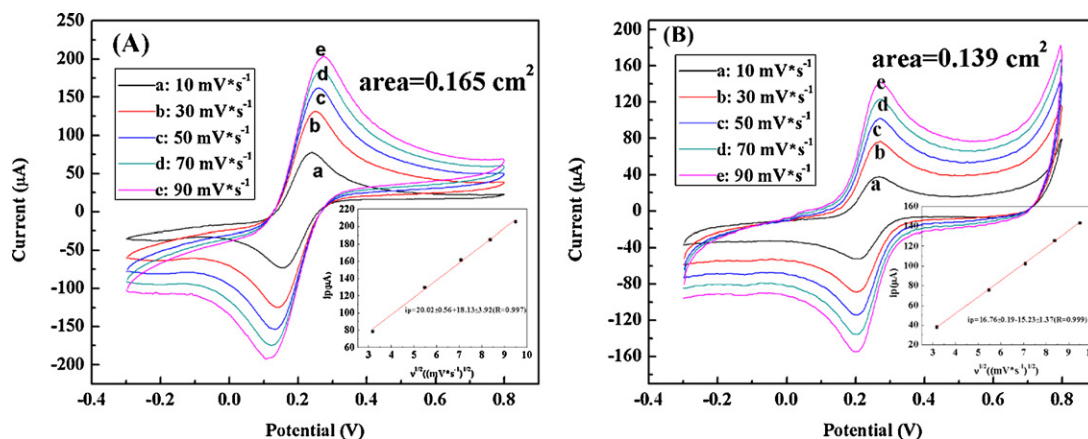


Fig. 5. CVs of the (A) Pt nanoflowers electrode and (B) Pt nanoparticles electrode in 5 mM $K_3[Fe(CN)_6]$ and 1 M KCl at different scan rates from inner to outer: 10, 30, 50, 70 and 90 $mV s^{-1}$. Inset of Fig. 5: Peak current as a function of scan rate for the determination of the electroactive surface area.

which indicated a quasi-reversible diffusion controlled process [38]. Therefore, under the temperature of 25 °C, the dependence of the peak current on the square root of the scan rate was described by the Randles-Sevcik equation:

$$I_p = 0.4463 \left(\frac{F^3}{RT} \right)^{1/2} n^{3/2} A D_0^{1/2} C_0 * \nu^{1/2} \quad (1)$$

where n represents the number of electrons participating in the redox reaction, ν was the scan rate ($V s^{-1}$), A was the electroactive area of the electrode (cm^2), D_0 was the diffusion coefficient of 5 mM $K_3[Fe(CN)_6]$ in 1 M KCl ($7.6 \times 10^{-6} cm^2 s^{-1}$), C_0 was the concentration of the probe molecule in the bulk solution ($mol cm^{-3}$), and I_p was the redox peak current (A) illustrated in Fig. 5. For $T = 298 K$ (25 °C): $0.4463(F^3/RT)^{1/2} = 2.687 \times 10^5 (mol V^{1/2})$. From this equation, the electroactive surface areas of the Pt nanoflowers and Pt nanoparticles electrode were calculated to be 0.165 cm^2 and 0.139 cm^2 , respectively.

EIS was a powerful technique for studying the interface properties of electrode surfaces [39]. Fig. 6 showed the typical Nyquist plots of the Pt nanoflowers electrode and Pt nanoparticles electrode. As observed in Fig. 6, for both Pt nanoflowers electrode and Pt nanoparticles electrode, a squeezed semicircle at high frequency, which corresponded to the electron transfer limited process, followed by a linear part at the low frequency attributable to diffusion controlled electron transfer process. In the low frequency region, no vertical increase in impedance on the imaginary part with decreasing the ac frequency was observed, which demon-

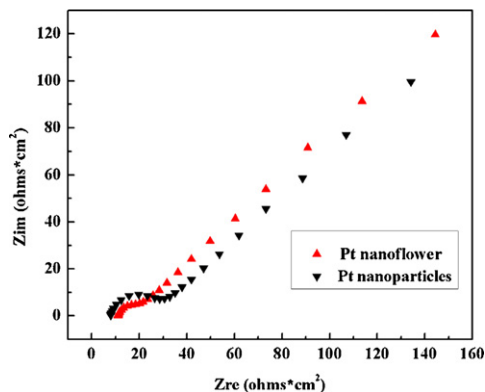


Fig. 6. Nyquist plots of the (a) Pt nanoflowers electrode and (b) Pt nanoparticles electrode in 5 mM $K_3[Fe(CN)_6]/K_4[Fe(CN)_6]$ and 0.1 M KCl solution.

strated that the electrodes showed no capacitive characteristics. The respective semicircle diameter at the high frequency equaled to the electron transfer resistance (R_{ct}) at the electrode surface. It was observed that the electron transfer resistance of the Pt nanoflowers electrode was about 15.06 Ωcm^2 , which was smaller than 31.08 Ωcm^2 of the Pt nanoparticles electrode. The results implied that the Pt nanoflowers electrode was more conductive to electron transfer than the Pt nanoparticles electrode.

Cyclic voltammetry was used to investigate the catalytic activities of the as-synthesized electrodes. Fig. S1 in Supplementary material showed CVs of the Pt nanostructured electrodes prepared at $-0.02 V$, $-0.2 V$ and $-0.6 V$ for 900 s in 20 mM glucose supported by 0.2 M neutral PBS. It was observed that the current response decreased in the order of Pt nanoflowers prepared at $-0.2 V >$ Pt nanoparticles prepared at $-0.02 V >$ Pt nanoparticles prepared at $-0.6 V$, which indicated that the Pt nanoflowers electrode possessed highest catalytic activity.

Fig. 7(A) showed CVs of Pt nanostructured electrodes prepared using (a) 0.5 M $H_2SO_4/3 mM H_2PtCl_6$ solution and (b) 0.5 M KCl/3 mM H_2PtCl_6 solution for 900 s in 20 mM glucose supported by 0.2 M neutral PBS. It was observed that the peak current density of glucose oxidation on Pt nanoflowers electrode ($14.80 \mu A cm^{-2}$) was about 4.9 times larger than that on Pt nanoparticles electrode ($2.54 \mu A cm^{-2}$). The strong response of the Pt nanoflowers electrode was resulted from large electroactive surface areas and small electron transfer resistance.

Fig. 7(B) showed CVs of the Pt nanoflowers electrode in blank solution (a), 20 mM glucose with the presence of 0.12 M NaCl (b) and without the presence of 0.12 M NaCl (c) supported by 0.2 M neutral PBS. As observed in Fig. 7(B), in the blank PBS solution, CVs was characterized by well-known hydrogen adsorption/desorption peaks at negative potentials, a flat double layer region at intermediate potentials, and platinum oxide formation and reduction peaks at positive potentials. The Pt nanoflowers electrode exhibited strong electrocatalytic activity to the glucose oxidation in the absence (curve b) and in the presence (curve c) of chloride ions at a very low potential of +0.03 V, and the peak current in the presence of chloride ions (curve c) was smaller than that without chloride ions (curve b). The oxidation of glucose and resulting intermediates were observed in the positive scan. Whereas in the negative scan, the oxidation of glucose was suppressed in the high potential range because of the presence of surface oxide, which was reduced at a potential of about +0.12 V. With the reduction of surface Pt oxide, more and more surface-active sites were available for the oxidation of glucose again, resulting in large and broad anodic peaks in the potential range from 0.0 to $-0.5 V$.

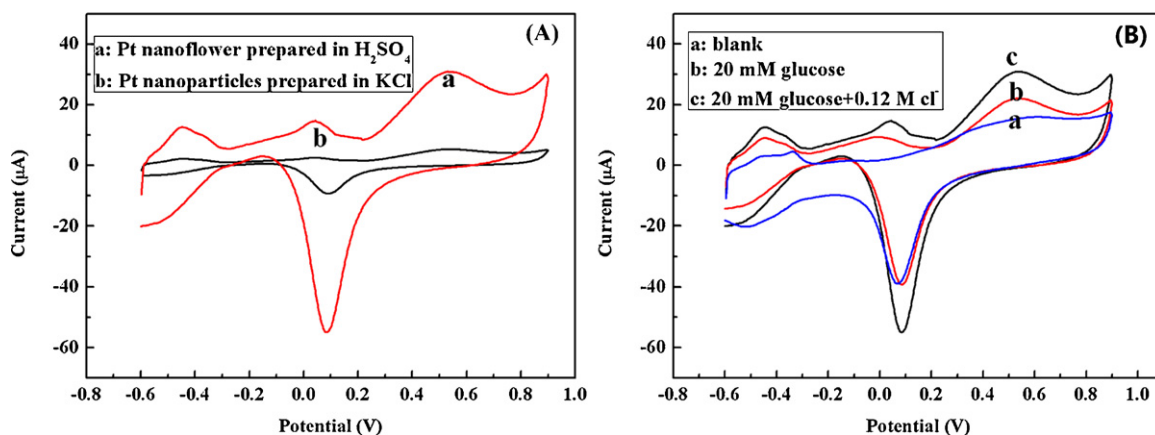


Fig. 7. (A) CVs of the (a) Pt nanoflowers electrode and (b) Pt nanoparticles electrode in 20 mM glucose supported by 0.2 M neutral PBS. (B) CVs of the Pt nanoflowers electrode in blank solution (a), 20 mM glucose with the presence of 0.12 M NaCl (b) and 20 mM glucose without the presence of 0.12 M NaCl (c) supported by 0.2 M neutral PBS.

3.3. Amperometric performance of the Pt nanoflowers electrode to glucose oxidation

Differential pulse voltammetry was used to determine the sensor outputs at different glucose concentrations. Fig. 8(A) represented the calibration curve for the determination of glucose at the Pt nanoflowers electrode. The measured peak current was found to be linearly proportional to the concentration of glucose in the solution in the range of 1–16 mM with a correlation coefficient of 0.9993, which covered the physiological level of 3–8 mM.

The detection limit of the sensor was 48 μM based on a signal-to-noise ratio of 3. Table 1 compared the performance of the reported enzyme-based glucose biosensors and nonenzyme sensors. As listed in Table 1, the detection limit, linear calibration range and sensitivity for glucose determination at the Pt nanoflowers electrode were comparable or even better than those obtained at several electrodes reported recently. An important analytical parameter for a sensor was its ability to discriminate between the interfering species commonly present in similar physiological environment. The interference from electroactive compounds,

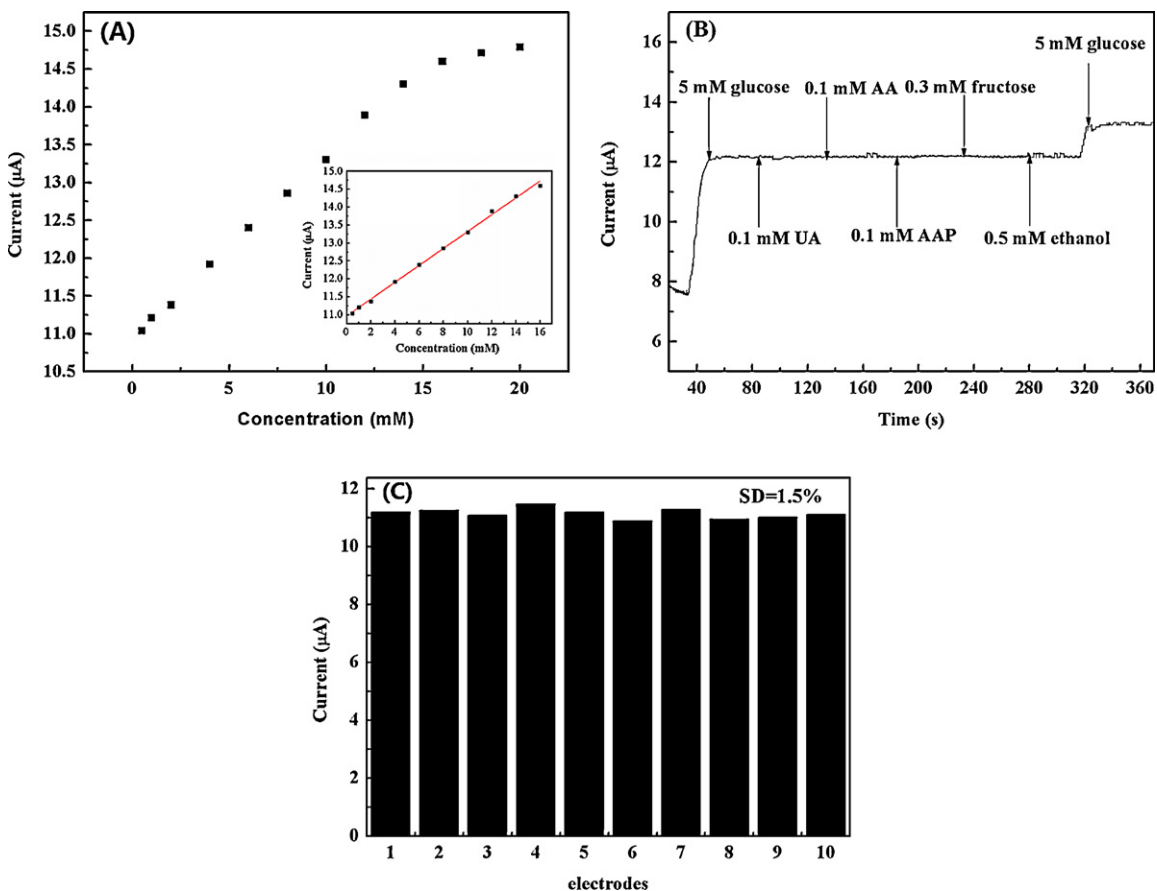


Fig. 8. (A) Calibration curve for the amperometric responses of the Pt nanoflowers electrode to glucose. Inset: the liner fit curve of current vs. concentration. (B) The influence of electroactive compounds (AA, UA, AAP, ethanol and fructose) on the response of 5.0 mM glucose in PBS (7.0). (C) Current response of 10 different Pt nanoflowers electrodes to 1.0 mM glucose in PBS (7.0).

Table 1
Analytical parameters obtained at different glucose sensors.

Electrode materials	Sensitivity	Linear range	Detection limit	Activity (Cl ⁻)
Pt nanotubules [17]	0.1 $\mu\text{A mM}^{-1} \text{cm}^{-2}$	2–14 mM	1 μM	Not applicable
Nanoporous Pt [40]	1.65 $\mu\text{A mM}^{-1} \text{cm}^{-2}$	1–10 mM	Not applicable	Not applicable
Mesoporous Pt [16]	9.6 $\mu\text{A cm}^{-2} \text{mM}^{-1}$ (+0.4 V)	Up to 10 mM	Not applicable	SCR ^a
Pt ₂ Pb [41]	Not applicable	Up to 15 mM	Not applicable	Not applicable
PtPb nanowires [20]	11.25 $\mu\text{A cm}^{-2} \text{mM}^{-1}$ (-0.2 V)	Up to 11 mM	8 μM	Not applicable
Au@Pd-ILs ^b -Au@Pd/GCE ^c [42]	0.00187 $\mu\text{A nM}^{-1}$ (0 V)	5 nM–0.5 μM	1 nM	Not applicable
SWCNHs ^d /GCE ^c [43]	1.06 $\mu\text{A mM}^{-1}$ (+0.3 V)	0–6 mM	6 μM	Not applicable
PtPbNP ^e /MWCN ^f /Ta [44]	18 $\mu\text{A mM}^{-1} \text{cm}^{-2}$ (-0.15 V)	1–5 mM	8 μM	Not applicable
Monodispersed Ni/Al layered Double hydroxide and chitosan [45]	0.182 $\mu\text{A mM}^{-1}$ (+0.9 V)	Up to 10 mM	10 μM	Not applicable
Nafion/OMCs ^g modified GE ^h [46]	0.053 $\mu\text{A mM}^{-1}$	0.5–15 mM	156.52 μM	Not applicable
ⁱ PS-PANI-Au-GOD [47]	Not applicable	0.04–2.04 mM	12 μM	Not applicable
^j GOx-AuNPs/ESM [48]	Not applicable	8.33 μM –0.966 mM	3.5 μM	Not applicable
This work	1.87 $\mu\text{A cm}^{-2} \text{mM}^{-1}$ (0.23 $\mu\text{A mM}^{-1}$) (+0.03 V)	1–16 mM	48 μM	SCR ^f

^a Strong current response.

^b Ionic liquids.

^c Glassy carbon electrodes.

^d Singlewalled carbon nanotubes.

^e Nanoparticles.

^f Multiwalled carbon nanotubes.

^g Ordered mesoporous carbons.

^h Graphite electrode.

ⁱ Polystyrene-polyaniline-Au-glucose oxidase nanocomposite.

^j Glucose oxidase-gold nanoparticles/eggshell membrane.

such as ascorbic acid (0.1 mM, AA), uric acid (UA, 0.1 mM), acetaminophenol (AAP, 0.1 mM) and fructose (0.3 mM), which commonly present in physiological samples, was investigated. In addition, the influence of ethanol (0.5 mM) on the response of 5.0 mM glucose was also investigated. From Fig. 8(B), it was observed that the response signals of AA, UA, fructose, ethanol and AAP were negligible for glucose determination. The good selectivity of the nonenzymatic sensor was related to the proper working potential used.

The reproducibility and stability of the nonenzymatic glucose sensor were evaluated via the comparison of the currents of different electrodes. The amperometric response of 10 different Pt nanoflowers electrodes to 1.0 mM glucose was tested independently. As shown in Fig. 8(C), the relative standard deviation (RSD) of the current response of the Pt nanoflowers electrode to 1 mM was 1.4% for 10 successive measurements. A reproducible current response with a RSD of 3.0% was observed for 30 successive assays of 1.0 mM glucose. The long-term stability was explored by measuring a glucose solution intermittently, and the electrode was stored at 4 °C by immersing in PBS (0.2 M, pH 7.0). The results showed that the catalytic current maintained more than 90% of its initial value after 30 days, indicating the good stability of the nonenzymatic glucose sensor.

4. Conclusions

A convenient and effective route to synthesize Pt nanoflowers on the surface of Au electrode was developed. The shape and size of the Pt nanoflowers were controlled by adjusting the deposition potential and time. The as-formed Pt nanoflowers were composed of metallic Pt. The electrochemical results demonstrated that Pt nanoflowers exhibited superior electrocatalytic performance towards the oxidation of glucose than the Pt nanoparticles. The as-prepared nonenzymatic glucose sensor exhibited good selectivity, stability and acceptable reproducibility for the determination of glucose. Because of the simple preparation method and good catalytic performance, such material has potential application in catalysis and sensor areas.

Acknowledgement

The authors gratefully acknowledge the support for this work from the National Natural Science Foundation of China (Grant 51143009).

Appendix A. Supplementary data

Supplementary data associated with this article can be found, in the online version, at doi:10.1016/j.electacta.2011.11.114.

References

- [1] E. Reitz, W.Z. Jia, M. Gentile, Y. Wang, Y. Lei, *Electroanalysis* 20 (2008) 2482.
- [2] Y.H. Lin, F. Lu, Y. Tu, Z.F. Ren, *Nano Lett.* 4 (2004) 191.
- [3] E.S. Forzani, H.Q. Zhang, L.A. Nagahara, I. Amlani, R. Tsui, N.J. Tao, *Nano Lett.* 4 (2004) 1785.
- [4] Y. Lin, L. Guodong, *Electrochem. Commun.* 8 (2006) 251.
- [5] S. Huang, Y. Ding, Y. Liu, L. Su, R. Filosa Jr., Y. Lei, *Electroanalysis* 23 (2011) 1912.
- [6] J. Wang, D.F. Thomas, A. Chen, *Anal. Chem.* 80 (2008) 997.
- [7] S. Park, H. Boo, T.D. Chung, *Anal. Chim. Acta* 556 (2006) 46.
- [8] B. Yu, S. Yingying, S. Changqing, *Biosens. Bioelectron.* (2008) 579.
- [9] F. Xiao, F.Q. Zhao, Y.F. Zhang, G.P. Guo, B.Z. Zeng, *J. Phys. Chem. C* 113 (2009) 849.
- [10] Y.B. Vassilyev, O.A. Khazova, N.N. Nikolaeva, *J. Electroanal. Chem.* 196 (1985) 105.
- [11] H. Zhu, X.Q. Lu, M.X. Li, Y.H. Shao, Z.W. Zhu, *Talanta* 79 (2009) 1446.
- [12] M.S. Celej, G. Rivas, *Electroanalysis* 10 (1998) 771.
- [13] E.Y.I.T. Baea, X. Xing, C.C. Liu, *J. Electroanal. Chem.* 309 (1991) 131.
- [14] H.M. Zhang, W.Q. Zhou, Y.K. Du, P. Yang, C.Y. Wang, *Electrochem. Commun.* 12 (2010) 882.
- [15] Q.M. Shen, L.P. Jiang, H. Zhang, Q.H. Min, W.H. Hou, J.J. Zhu, *J. Phys. Chem. C* 112 (2008) 16385.
- [16] S. Park, T.D. Chung, H.C. Kim, *Anal. Chem.* 75 (2003) 3046.
- [17] J.H. Yuan, K. Wang, X.H. Xia, *Adv. Funct. Mater.* 15 (2005) 803.
- [18] Y.Y. Song, D. Zhang, W. Gao, X.H. Xia, *Chem. Eur. J.* 11 (2005) 2177.
- [19] K.T.M. Sakamoto, *Bioelectrochemistry* 9 (1982) 571.
- [20] Y. Bai, Y.Y. Sun, C.Q. Sun, *Biosens. Bioelectron.* 24 (2008) 579.
- [21] H.F. Cui, J.S. Ye, X. Liu, W.D. Zhang, *Nanotechnology* 17 (2006) 2334.
- [22] X. Zhang, K.-Y. Chan, J.-K. You, Z.-G. Lin, A.C.C. Tseung, *J. Electroanal. Chem.* 430 (1997) 147.
- [23] P. Holt-Hindle, Q.F. Yi, G.S. Wu, K. Koczur, A.C. Chen, *J. Electrochem. Soc.* 155 (2008) K5.
- [24] L.Z. Zheng, L.Y. Xiong, J. Sun, J.H. Li, S.M. Yang, J. Xia, *Catal. Commun.* 9 (2008) 624.
- [25] G. Demazeau, *J. Mater. Sci.* 43 (2008) 2104.
- [26] J.Y. Kim, Z.G. Yang, C.C. Chang, T.I. Valdez, S.R. Narayanan, P.N. Kumta, *J. Electrochem. Soc.* 150 (2003) A1421.

- [27] M.H. Yang, Y.H. Yang, Y.L. Liu, G.L. Shen, R.Q. Yu, *Biosens. Bioelectron.* 21 (2006) 1125.
- [28] H. Kawasaki, T. Yonezawa, T. Watanabe, R. Arakawa, *J. Phys. Chem. C* 111 (2007) 16278.
- [29] X.Y. Hu, D.G. Cahill, R.S. Averback, *Appl. Phys. Lett.* 76 (2000) 3215.
- [30] L.C. Nagle, J.F. Rohan, *J. Power Sources* 185 (2008) 411.
- [31] J.T. Zhang, H.Y. Ma, D.J. Zhang, P.P. Liu, F. Tian, Y. Ding, *Phys. Chem. Chem. Phys.* 10 (2008) 3250.
- [32] K.S. Napolskii, P.J. Barczuk, S.Y. Vassiliev, A.G. Veresov, G.A. Tsirlina, P.J. Kulesza, *Electrochim. Acta* 52 (2007) 7910.
- [33] S.Z. Chu, H. Kawamura, M. Mori, *J. Electrochem. Soc.* 155 (2008) D414.
- [34] A.C. Chen, P. Holt-Hindle, *Chem. Rev.* 110 (2010) 3767.
- [35] L.A. Su, W.Z. Jia, L.C. Zhang, C. Beacham, H. Zhang, Y. Lei, *J. Phys. Chem. C* 114 (2010) 18121.
- [36] F. Xiao, Z.R. Mo, F.Q. Zhao, B.Z. Zeng, *Electrochem. Commun.* 10 (2008) 1740.
- [37] A. Eftekhari, *J. Electrochem. Soc.* 151 (2004) E291.
- [38] A.S. Baranski, T. Krogulec, L.J. Nelson, P. Norouzi, *Anal. Chem.* 70 (1998) 2895.
- [39] M. Guo, H. Fang, R. Wang, Z. Yang, X. Xu, *J. Mater. Sci. Mater. Med.* 22 (2011) 1985.
- [40] S. Joo, S. Park, T.D. Chung, H.C. Kim, *Anal. Sci.* 23 (2007) 277.
- [41] Y.P. Sun, H. Buck, T.E. Mallouk, *Anal. Chem.* 73 (2001) 1599.
- [42] X. Chen, H. Pan, H. Liu, M. Du, *Electrochim. Acta* 56 (2010) 636.
- [43] X. Liu, L. Shi, W. Niu, H. Li, G. Xu, *Biosens. Bioelectron.* 23 (2008) 1887.
- [44] H.F. Cui, J.S. Ye, W.D. Zhang, C.M. Li, J.H.T. Luong, F.S. Sheu, *Anal. Chim. Acta* 594 (2007) 175.
- [45] H. Ai, X. Huang, Z. Zhu, J. Liu, Q. Chi, Y. Li, Z. Li, X. Ji, *Biosens. Bioelectron.* 24 (2008) 1048.
- [46] M. Zhou, L. Shang, B. Li, L. Huang, S. Dong, *Biosens. Bioelectron.* 24 (2008) 442.
- [47] Y. Liu, X. Feng, J. Shen, J.J. Zhu, W. Hou, *J. Phys. Chem. B* 112 (2008) 9237.
- [48] B. Zheng, S. Xie, L. Qian, H. Yuan, D. Xiao, M.M.F. Choi, *Sens. Actuators B: Chem.* 152 (2011) 49.